

# Journal of Geophysical Research: Atmospheres

## RESEARCH ARTICLE

10.1002/2017JD026575

**Key Points:**

- North Pacific atmospheric high pressure similar to that responsible for the 2013–2016 California drought linked to unusual ocean conditions
- Simulations from climate model ensemble reproduce observed relationships between Pacific Ocean temperatures and atmospheric circulation
- Autumn sea surface temperatures, particularly in the tropical western Pacific Ocean, may enhance foresight of anomalous West Coast winter ridging

**Supporting Information:**

- Supporting Information S1
- Figure S1
- Figure S2
- Figure S3
- Figure S4
- Figure S5
- Figure S6

**Correspondence to:**D. L. Swain,  
dlswain@ucla.edu**Citation:**

Swain, D. L., Singh, D., Horton, D. E., Mankin, J. S., Ballard, T. C., & Diffenbaugh, N. S. (2017). Remote linkages to anomalous winter atmospheric ridging over the northeastern Pacific. *Journal of Geophysical Research: Atmospheres*, 122, 12,194–12,209. <https://doi.org/10.1002/2017JD026575>

Received 31 JAN 2017

Accepted 20 OCT 2017

Accepted article online 24 OCT 2017

Published online 24 NOV 2017

## Remote Linkages to Anomalous Winter Atmospheric Ridging Over the Northeastern Pacific

Daniel L. Swain<sup>1,2</sup> , Deepti Singh<sup>1,3</sup> , Daniel E. Horton<sup>4</sup> , Justin S. Mankin<sup>3,5</sup> , Tristan C. Ballard<sup>1</sup>, and Noah S. Diffenbaugh<sup>1,6</sup> 

<sup>1</sup>Department of Earth System Science, Stanford University, Stanford, CA, USA, <sup>2</sup>Institute of the Environment and Sustainability, University of California, Los Angeles, CA, USA, <sup>3</sup>Lamont-Doherty Earth Observatory, Columbia University, Palisades, NY, USA, <sup>4</sup>Department of Earth and Planetary Sciences, Northwestern University, Evanston, IL, USA, <sup>5</sup>NASA Goddard Institute for Space Studies, New York, NY, USA, <sup>6</sup>Woods Institute for the Environment, Stanford University, Stanford, CA, USA

**Abstract** Severe drought in California between 2013 and 2016 has been linked to the multiyear persistence of anomalously high atmospheric pressure over the northeastern Pacific Ocean, which deflected the Pacific storm track northward and suppressed regional precipitation during California's winter "rainy season." Multiple hypotheses have emerged regarding why this high pressure ridge near the west coast of North America was so resilient—including unusual sea surface temperature patterns in the Pacific Ocean, reductions in Arctic sea ice, random atmospheric variability, or some combination thereof. Here we explore relationships between previously documented atmospheric conditions over the North Pacific and several potential remote oceanic and cryospheric influences using both observational data and a large ensemble of climate model simulations. Our results suggest that persistent wintertime atmospheric ridging similar to that implicated in California's 2013–2016 drought can at least partially be linked to unusual Pacific sea surface temperatures and that Pacific Ocean conditions may offer some degree of cool-season foresight in this region despite the presence of substantial internal variability.

**Plain Language Summary** Severe drought in California between 2013 and 2016 has previously been linked to the persistence of atmospheric high atmospheric pressure over the Pacific Ocean (nicknamed the "Ridiculously Resilient Ridge"), which prevented winter storms from reaching the coast over several consecutive years. There has been much discussion regarding why this high-pressure system has been so persistent—and some scientists have previously suggested that unusual ocean temperature patterns in the Pacific, reductions in Arctic sea ice, or random weather variations may have played a role. In this study, we investigate relationships between atmospheric high pressure over the North Pacific and possible links to ocean conditions using both real-world observations and climate model simulations. Our results suggest that persistent atmospheric high pressure similar to that which occurred during California's 2013–2016 drought can be partially linked to unusual Pacific Ocean temperatures and that knowledge of such ocean conditions may offer foresight regarding the potential for future droughts in this region.

### 1. Introduction

California experienced a severe drought beginning in early 2013, with substantial consequences for California's heavily managed water supply (Swain, 2015). Due to the prolonged nature of this extreme event, adverse environmental impacts were especially pronounced—including widespread forest mortality (Asner et al., 2016), increased wildfire activity (Yoon et al., 2015), and the near extirpation of certain aquatic species in the most affected watersheds (Jeffries et al., 2016). From a physical climate perspective, the magnitude of California's multiyear drought was unprecedented in the direct instrumental (Swain et al., 2016) and short-term proxy records (Griffin & Anchukaitis, 2014), bringing both the lowest mountain snowpack in 500 years (Belmecheri et al., 2016) and the most extreme combination of high temperatures and low precipitation in at least a millennium (Griffin & Anchukaitis, 2014; Robeson, 2015).

These large cumulative precipitation deficits and record-high temperatures were associated with the multiyear persistence of atmospheric high pressure over the northeastern Pacific Ocean during California's October-to-May wet season (Seager et al., 2015; Swain, 2015; Swain et al., 2014; H. Wang & Schubert, 2014; Wang et al., 2014). This so-called "Ridiculously Resilient Ridge" (Swain et al., 2014) brought about a

recurring northward deflection of the North Pacific storm track and disrupted the typically well-defined seasonal cycle (Swain et al., 2016) in California's "Mediterranean" climate zone (Cayan & Roads, 1984). Though its structure and spatial orientation varied considerably over the course of the drought, the longevity and overall coherence of this striking atmospheric feature over successive winters was nonetheless unprecedented in the observational record (Swain et al., 2014).

While it is very likely that the human emission of greenhouse gases is at least partially responsible for the record-breaking warmth during the 2013–2016 California drought (Diffenbaugh, Swain, & Touma, 2015), and therefore the drought's overall intensity (Griffin & Anchukaitis, 2014; Robeson, 2015; Williams et al., 2015), there remains considerable uncertainty regarding the physical causes underlying the persistence of North Pacific high pressure (Hartmann, 2015; Lee et al., 2015; Seager et al., 2015; Wang et al., 2014). A reasonable null hypothesis is that this anomalous high-pressure "ridging" is the product of internal variability: that the atmospheric anomaly (and associated precipitation deficits) arose largely at random, without direct forcing by conditions in the broader Earth system (Seager et al., 2015). However, recent studies hint at a more traceable etiology, with evidence of remote teleconnections to North Pacific ridging via tropical excitation of atmospheric Rossby waves (Hartmann, 2015; Lee et al., 2015; Seager & Henderson, 2016; Teng & Branstator, 2016; Wang et al., 2014). Other studies have hinted that the thermally direct (or indirect) effects of Arctic sea ice loss (Lee et al., 2015; Overland et al., 2016; Pedersen et al., 2016) may also play a role in North Pacific atmospheric variability, though a well-defined mechanism remains elusive. There is also observational evidence that seasonally persistent North Pacific high-pressure patterns similar to those which occurred during the 2013–2014 and 2014–2015 winter seasons have occurred more frequently in recent decades, coincident with a regional maximum of lower tropospheric warming along the west coast of North America (Swain et al., 2016). Collectively, these previous findings raise the possibility that unusual remote ocean temperatures (and perhaps sea ice conditions) may have contributed to the anomalous North Pacific/North American atmospheric conditions during 2013–2016.

Motivated by this recent work, we use observational data and climate model experiments to explore potential linkages between northeastern Pacific atmospheric conditions and regional sea surface temperature (SST) and Arctic sea ice extent (SIE). We focus on ocean and ice conditions associated with anomalous atmospheric ridging in the storm track region immediately to the west of California, which is strongly linked to the occurrence of dry conditions on seasonal to annual timescales (Swain et al., 2014). In this analysis, we investigate observed empirical relationships among five potential remote influences and an atmospheric response variable (the 500 hPa geopotential height (GPH) field via multiple linear regression. The five potential remote influences are SST anomalies in the tropical western Pacific (WP), tropical eastern Pacific (EP) and extratropical northeastern Pacific (NEP), and SIE anomalies in the Barents/Kara (BK) and Bering/Chukchi (BC) regions. (See section 2 for details regarding implementation and regressor selection.) We use a large ensemble of climate model simulations to assess whether observed relationships are likely the products of internal atmospheric variability alone or plausibly represent robust Earth system linkages that may yield insights into the underlying causes of atmospheric ridging conducive to drought in California.

## 2. Methods

### 2.1. Selection of Remote Regressors

We seek to explore relationships between sea surface temperature/sea ice extent (SST/SIE) in specific Northern Hemisphere regions and atmospheric conditions over the North Pacific. We stress that our methods do not allow us to make explicit claims regarding the direction of causality involved in these relationships—instead, we investigate statistical linkages between the surface and atmospheric conditions in geographically distant regions. Further study will be required to more clearly elucidate underlying mechanisms, though the temporally lagged relationships we investigate offer insights into the persistence of ocean-atmosphere interactions on multimonth timescales.

Selection of SST and SIE regressors is directly informed by mechanistic hypotheses set forth in the existing literature—including well-known modes of variability and associated teleconnection patterns. Our EP region was chosen primarily to represent the effect of the El Niño–Southern Oscillation (ENSO) in the tropical and lower latitude subtropical eastern Pacific (and, indeed, we confirm that SST in the EP region exhibits its highest values during 1982–1983, 1997–1998, and 2015–2016—coinciding with the three most powerful El Niño

events on record). The effects of ENSO upon West Coast precipitation have been described extensively, although recent work has increasingly focused on the diversity of ENSO teleconnections (Hoell et al., 2016), which appear to depend on the overall structure of SST anomalies in the North Pacific (Hoell & Funk, 2013). Our WP region is intended to capture the potential atmospheric response to western tropical Pacific SST variability unrelated to ENSO, which has been directly implicated by at least some studies in the persistence of recent northeastern Pacific high pressure (Hartmann, 2015; Lee et al., 2015; Seager & Henderson, 2016; Wang et al., 2014), and is more generally linked to an increased risk of extreme winter ridging near the West Coast of North America (Teng & Branstator, 2016). Additionally, there is evidence that SSTs in this region may modulate increased ENSO- and ENSO-precursor-related atmospheric variability over the North Pacific under 21st century global warming scenarios, potentially leading to both increased dry and wet seasonal precipitation extremes in California (Yoon et al., 2015).

We include NEP SST in our analysis in response to enhanced interest in the North Pacific “Blob” (Bond et al., 2015)—a persistent region of extraordinarily warm SST that has coincided in time and space with anomalous high pressure in the overlying atmosphere. While recent warm SST in the “Blob” region is thought to be primarily a second-order response to atmospheric high pressure via reduced sea-air energy fluxes associated with storm track suppression (Bond et al., 2015; Di Lorenzo & Mantua, 2016), there is also evidence that global warming has substantially increased the likelihood of extreme northeastern Pacific SST (Di Lorenzo & Mantua, 2016; Funk, Hoell, & Stone, 2014) and that resultant lower tropospheric temperatures could act to amplify the preexisting atmospheric standing wave pattern along the West Coast (Swain et al., 2016). It is also possible that record-warm SSTs in this region could be associated with a tropically induced excitation of the North Pacific Mode during the early part of the drought (Hartmann, 2015) or with the increasingly positive phase of the Pacific Decadal Oscillation during 2015 (Di Lorenzo & Mantua, 2016). While previous evidence suggests that NEP SST is unlikely to have been an initial trigger of anomalous ridging during the recent California drought (Bond et al., 2015; Hartmann, 2015; Seager et al., 2015), we include it in our analytical framework primarily due to the potential for strong ocean-atmosphere feedback on multimonth timescales in the extratropical North Pacific (Di Lorenzo & Mantua, 2016; Fang & Yang, 2016; Gan & Wu, 2012; Lee et al., 2015).

Finally, our selection of geographically distinct BK and BC SIE domains (as opposed to a pan-Arctic mean) stems from recent studies showing pointedly different midlatitude responses to sea ice loss in different regions (Kug et al., 2015; Pedersen et al., 2016). In particular, recent work has linked sea ice loss in the BK region in particular to a weakened polar vortex (Zhang et al., 2016), which has been shown to have substantial effects upon the lower tropospheric circulation over North America during winter (Kug et al., 2015). However, the spatial character of the regional response to sea ice loss (for example, the “Warm Arctic/Cold Continents” pattern) and its magnitude relative to large natural variability remains the subject of considerable uncertainty (Shepherd, 2016)—emphasizing the importance of considering each region separately. While there is limited direct evidence that sea ice conditions contributed to the anomalous atmospheric conditions during the California drought period specifically (Lee et al., 2015), recent studies suggest that 21st century sea ice loss may strongly affect the strength and position of the North Pacific storm track (e.g., Blackport & Kushner, 2017; Overland et al., 2016; Pedersen et al., 2016), which would have substantial implications for California seasonal precipitation.

## 2.2. Construction of Statistical Model

In our analysis, we construct multiple linear regression models of the form

$$Y = \beta_0 + \beta_1 X_1 + \beta_2 X_2 + \beta_3 X_3 + \beta_4 X_4 + \beta_5 X_5 + \beta_6 X_6$$

where  $Y$  represents the atmospheric response variable (i.e., GPH (m)),  $X_1 - 5$  represent standardized SST/SIE values (mean = 0, standard deviation = 1),  $\beta_0$  represents the intercept term,  $\beta_1 - 5$  represent standardized regression coefficients for SST/SIE regressors, and  $\beta_6$  represents a “year term” to account for any linear trend in the response. Standardized regression coefficients allow for more direct comparisons between the respective magnitudes of effects that different regressors have on the atmospheric response.

We create regressions for GPH on a gridbox-by-gridbox basis—building separate linear regressions that estimate the atmospheric response variable at each location in the Northern Hemisphere. We also create separate linear regressions for both observational and climate model data (Figures 1, 2, S1, and S2 in the

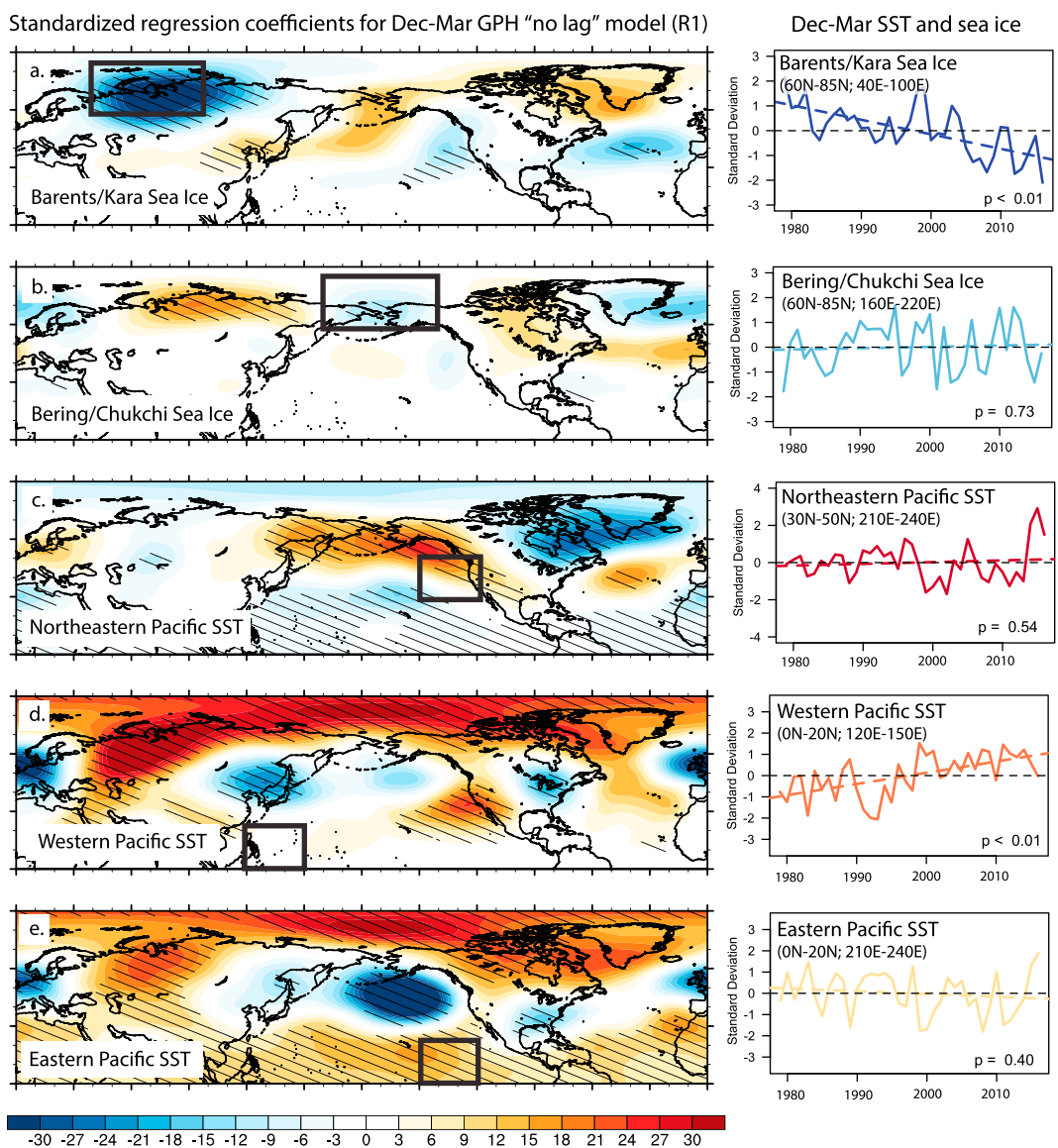


**Figure 1.** (a–e) Observed relationships between December–March (no lag) SST/SIE regressors and December–March atmospheric conditions (NCEP/NCAR R1 Reanalysis). (left column) Standardized regression coefficients for 500 hPa geopotential height anomalies (color shading; units = m). The hashed regions denote areas where regression coefficients are statistically significant at or below  $p = 0.10$ . The black rectangles on map depict geographic region corresponding to each regressor. (right column) Time series of observed December–March regressor values for 1979–2016 (ERSSTv4 and HadISST). The dashed trend lines depict linear time trends from simple linear regression.  $P$  values denote statistical significance of linear trend during full period of record.

supporting information). In constructing our observational model, we use GPH data from the National Centers for Environmental Prediction/National Center for Atmospheric Research (NCEP/NCAR) R1 Reanalysis (Kalnay et al., 1996), SST data from the NOAA Extended Reconstructed Sea Surface Temperature Version 4 (ERSSTv4) data set (Huang et al., 2014), and SIE from the Hadley Centre Sea Ice and Sea Surface Temperature (HadISST) data set (Rayner et al., 2003) for each year between 1979 and 2012 (Figure 3a). For our climate model analysis, we use simulated GPH, SST, and SIE data from the Community Earth System Model (CESM) Large Ensemble Experiment (CESM-LE) (Kay et al., 2015). We examine data from 28 separate CESM-LE ensemble members, creating separate regressions for each realization to accommodate the possibility that simulated internal variability gives rise to divergent relationships across the ensemble. These members differ only by their initial atmospheric conditions in 1920 and are each

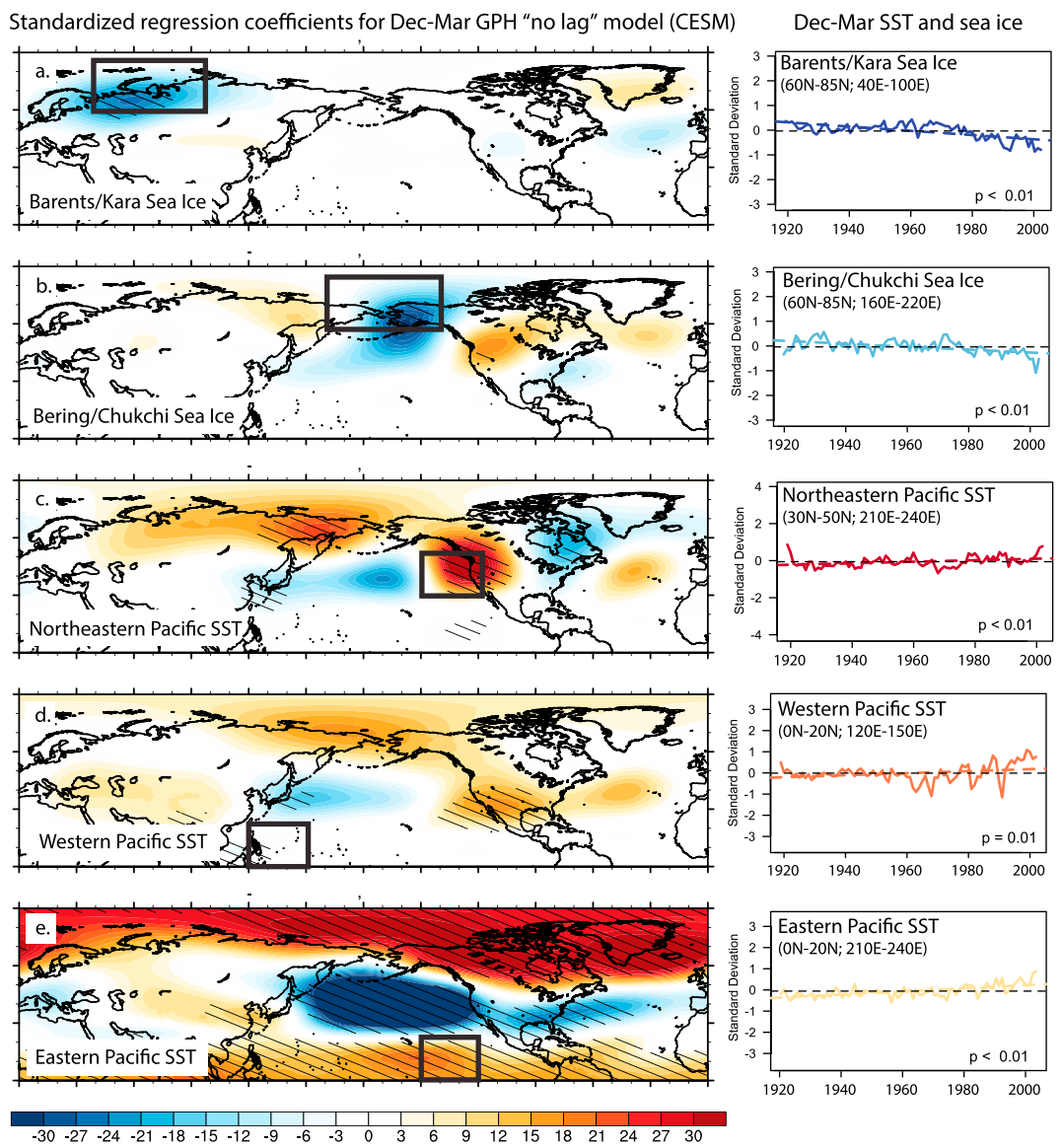


**Figure 2.** (a–e) Simulated relationships between December–March (no lag) SST/SIE regressors and December–March atmospheric conditions (CESM Large Ensemble Experiment). (left column) Standardized regression coefficients for 500 hPa geopotential height anomalies (color shading; units = m). The hashed regions denote areas where regression coefficients are statistically significant at or below  $p = 0.10$ . The black rectangles on map depict geographic region corresponding to each regressor. (right column) Time series of observed December–March regressor values for 1979–2016. The dashed trend lines depict linear time trends from simple linear regression.  $P$  values denote statistical significance of linear trend during full period of record.

forced with the same historical time series of atmospheric constituent concentrations between 1920 and 2005.

We emphasize that our primary goal in constructing each of these statistical models is to assess the character and spatial patterns of relationships between remote regressors and atmospheric conditions during the severe 2013–2016 California drought. We construct separate statistical models that incorporate both temporally simultaneous ("contemporaneous") and temporally lagged regressor values. We use December–March SIE and SST values to estimate contemporaneous December–March GPH (henceforth the "no lag" model), and September–November SIE and SST values to estimate December–March GPH values (henceforth the "lag" model). We choose to focus on atmospheric conditions during December–March in both cases as

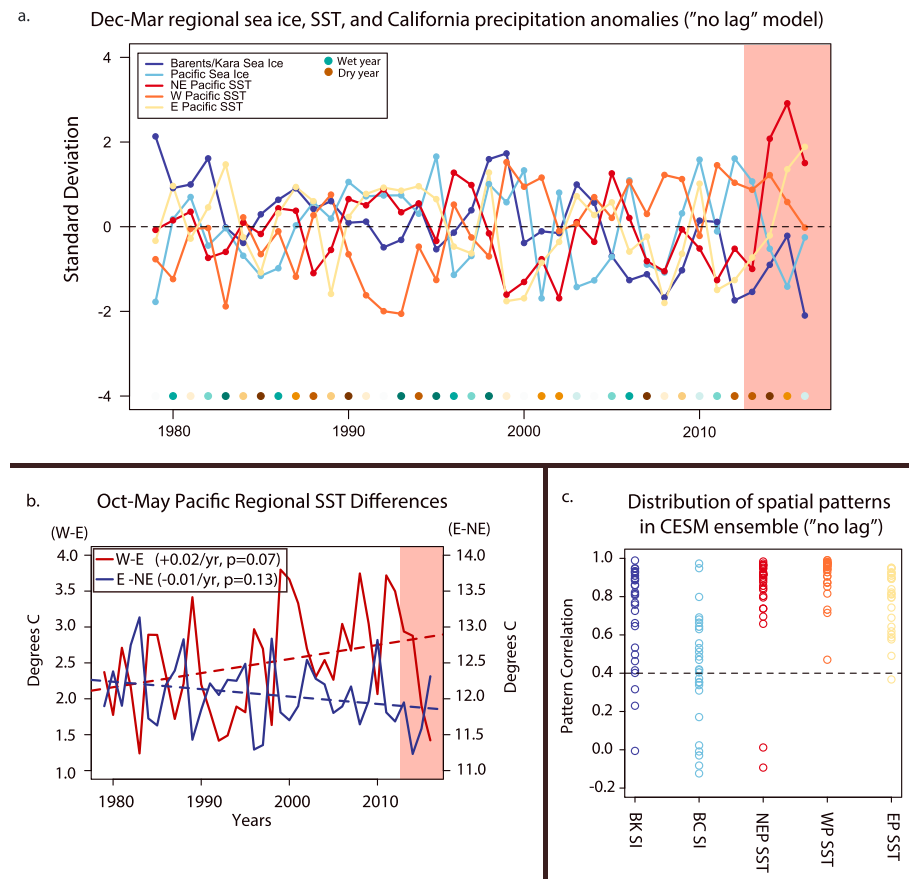


**Figure 3.** Character of relationships between Earth system regressors and North Pacific atmospheric circulation. (a) Combined time series of all December–March sea surface temperature and sea ice extent regressors used in this study (colored lines and points). The blue (brown) points near the bottom of the figure represent observed December–March California wet (dry) precipitation anomalies (binned by percentile in increments of 10%). (b) Time series of October–May regional Pacific sea surface temperature gradients. The red (blue) lines depict the difference between the tropical West and tropical East Pacific (tropical East Pacific and extratropical northeastern Pacific). The dashed lines represent the linear trend for each regional gradient between 1979 and 2016 ( $^{\circ}\text{C}/\text{yr}$ ).  $P$  values denote significance of each trend. Note the different y axes for each time series. (c) Similarity of North Pacific geopotential height anomaly pattern for each regressor between each of 28 CESM-LENS ensemble members and the unweighted ensemble mean (using the December–March no lag model). The red shaded regions in all time series represent the 2013–2016 California drought period.

these months constitute the peak of the California “wet season” (Cayan & Roads, 1984; Swain et al., 2016), and the period during which the climatological mean West Coast winter mean ridge reaches its maximum amplitude (Swain et al., 2016). We present the full range of results using the both the lag and no lag formulations for reanalysis and climate model data.

The unusually large number of ensemble members (and the wide range of simulated internal ocean/climate variability) in CESM-LE provides a unique opportunity to increase the effective “sample size” of our analysis, thereby allowing us to assess whether the observed relationships between SST/SIE and North Pacific atmospheric conditions are statistically robust and/or physically plausible (Figures 3c and 4). Recent work has shown that natural variability can lead to substantial and statistically significant trends in regional atmospheric circulation over decades (Deser et al., 2014; Horton et al., 2015) and that separating the relative role of climate change can be challenging (Horton et al., 2015; Shepherd, 2014; Singh et al., 2016). An important caveat, however, is that CESM is only a single coupled ocean-atmosphere model, and any systematic biases that the model may exhibit are propagated into our results. This is especially relevant for the complex Earth system feedback involved in sea ice-related teleconnections, which global climate models like CESM may struggle to adequately represent (Zhang et al., 2016).

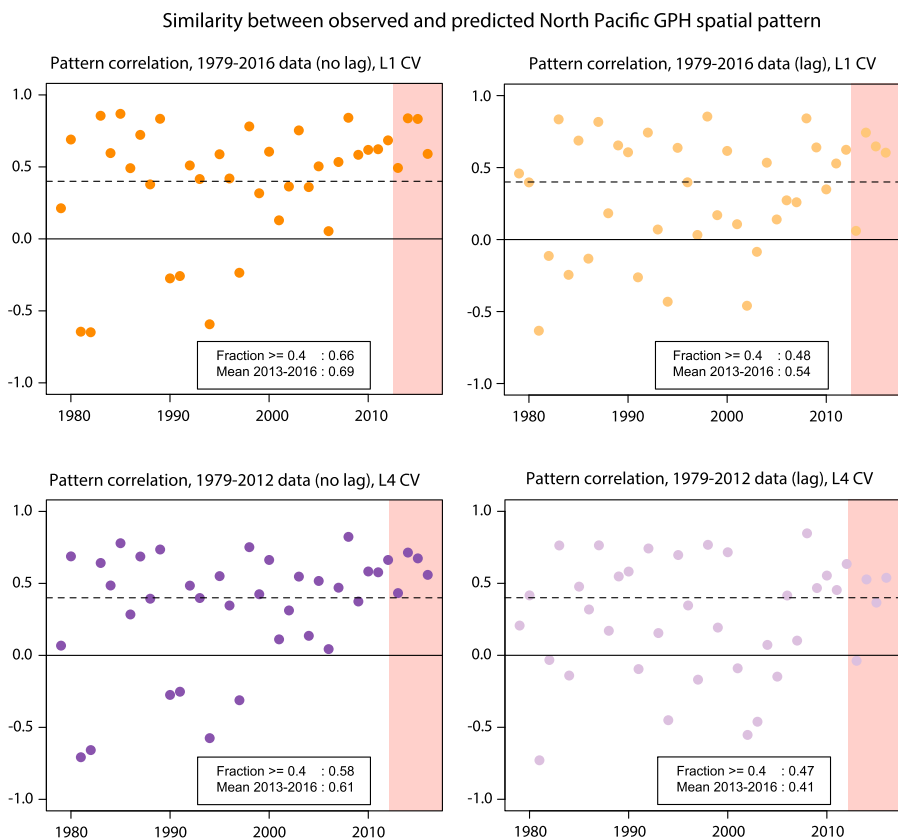


**Figure 4.** Cross-validation results for December–March no lag model (dark orange and dark purple points) and September–November lag model (light orange and light purple points). (top row) Results using a systematic leave one out approach, using a model trained on all data between 1979 and 2016 except for the single validation year. (bottom row) Results using a bootstrapped ( $n = 1000$ ) leave four out approach, using a model trained using data between 1979 and 2012 (i.e., excluding all data from 2012 to 2016 and four random training years). Metric of assessment is the anomaly pattern correlation between observed and estimated 500 hPa geopotential height anomalies in the northeastern Pacific. Also noted is the overall fraction of estimations that yielded “moderate to high” pattern correlation ( $\geq 0.4$ ) during cross validation and the mean similar for the 2013–2016 drought years of interest.

Prior to analysis, we create regional SST and SIE time series for both observational and climate model data by calculating latitude-weighted aerial means in the following geographic regions (see Figures 1 and 2 for map representation): Barents/Kara (BK) ( $60^{\circ}\text{N}$ – $85^{\circ}\text{N}$ ,  $40^{\circ}\text{E}$ – $100^{\circ}\text{E}$ ), Bering/Chukchi (BC) ( $60^{\circ}\text{N}$ – $85^{\circ}\text{N}$ ,  $160^{\circ}\text{E}$ – $220^{\circ}\text{E}$ ), northeastern Pacific (NEP) ( $30^{\circ}\text{N}$ – $50^{\circ}\text{N}$ ,  $210^{\circ}\text{E}$ – $240^{\circ}\text{E}$ ), West Pacific (WP) ( $0^{\circ}\text{N}$ – $20^{\circ}\text{N}$ ,  $130^{\circ}\text{E}$ – $160^{\circ}\text{E}$ ), and East Pacific (EP) ( $0^{\circ}\text{N}$ – $20^{\circ}\text{N}$ ,  $210^{\circ}\text{E}$ – $240^{\circ}\text{E}$ ). Gridboxes with sea ice concentration  $>50\%$  are considered “ice covered” and are included in extent calculations.

In all CESM analyses, each model realization is treated separately until the final step—meaning that 28 separate regressions and SST/SIE time series are generated. From these, we generate unweighted ensemble-mean regression coefficients and time series. We note that the CESM-LENS “Historical” forcing simulations used in this study only extend to 2005 and therefore do not fully overlap with the 1979–2016 observational period. Significant differences between real-world and prescribed aerosol forcings (especially volcanic contributions) in the corresponding post-2005 Representative Concentration Pathway simulations (Medhaug et al., 2017; Santer et al., 2014) make direct comparison of specific regional climate patterns difficult. As a result, we restrict our model analysis to the Historical simulations up through 2005, while also acknowledging that a modest amount of additional greenhouse gas forcing occurred between 2005 and 2016.

### 2.3. Model Cross Validation and California Drought Assessment

We assess the fidelity of our empirical models by calculating the anomaly pattern correlation between the regression-estimated and observed GPH field in the North Pacific Domain ( $25^{\circ}\text{N}$ – $55^{\circ}\text{N}$ ,  $200^{\circ}\text{E}$ – $250^{\circ}\text{E}$ ;

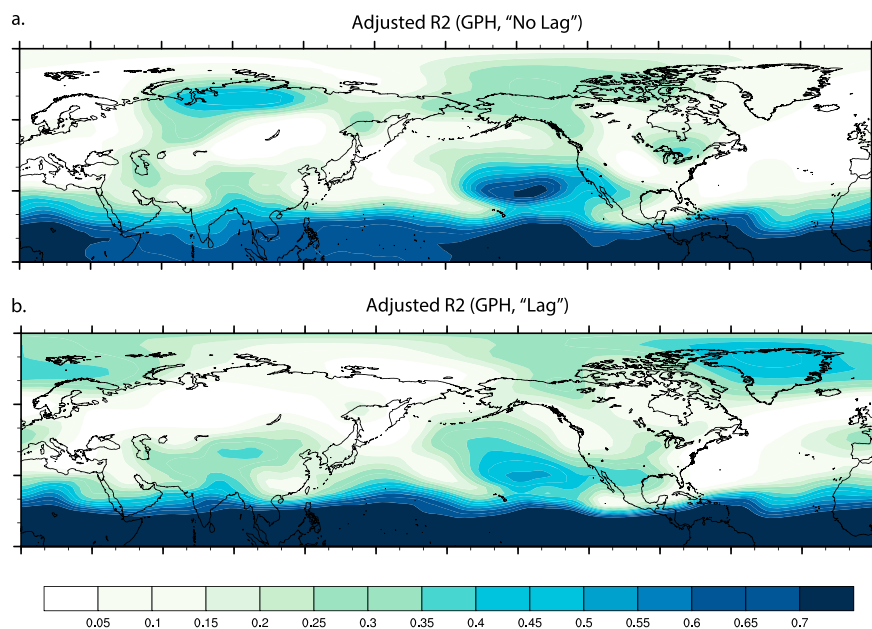


**Figure 5.** Adjusted  $R^2$  values for observational (R1 NCEP/NCAR Reanalysis) model: (top) December–March no lag model and (bottom) September–November lag model, with larger values suggesting a better fit to the data.

Figures 4–6). This region includes far western continental North America and the adjacent Pacific storm track offshore—encompassing the region through which virtually all precipitation-bearing storm systems affecting California pass (Swain et al., 2016). We use 500 mb GPH anomaly pattern correlation as a primary metric of model performance, as it provides a quantitative measure of spatial “likeness” to specific anomalous atmospheric patterns of interest (i.e., those occurring between 2013 and 2016), and because the magnitude/distribution of GPH itself integrates the thermodynamic characteristics of the entire lower troposphere (e.g., Swain et al., 2016). We define “moderate to high” pattern similarity as pattern correlation  $\geq 0.4$ , as this threshold has previously been used to objectively identify seasonally persistent North Pacific ridges (Swain et al., 2016).

To assess the sensitivity of our empirical regression models to the inclusion of training data, we perform two sets of comprehensive cross validation. We first conduct “leave-one-out” cross validation on the contemporaneous and temporally leading empirical models. In both cases, we train 38 different multiple linear regressions using subsets of training data that each excludes a single year of regressor values between 1979 and 2016. Statistical model performance is then assessed in all 38 instances by comparing model estimations with observations during the single excluded year—effectively generating an “out of sample” test for a single year in each model formulation. As a metric of model “goodness of fit” and stability over time, we again calculate the 500 mb GPH anomaly pattern correlation between the out-of-sample estimations and the observations (as described above).

We subsequently take a more restrictive cross-validation approach, conducting “leave-four-out” cross validation using both the contemporaneous and temporally leading data for the years between 1979 and 2012. Here we create random 30 year subsamples of the 34 years of data between 1979 and 2012 using a bootstrap resampling approach ( $n = 1,000$ ). We fit separate regressions to each of the 1,000 subsamples of the empirical data, once again assessing model performance using the GPH pattern correlation metric discussed previously. We note that this “leave four out approach” effectively yields an “out of sample” test for eight separate years in each iteration: the four randomly excluded years in the subsample, plus the four California drought years between 2013 and 2016 that are excluded from the training set in every iteration. We report the results of both cross validation methods side by side in Figure 4.

Finally, we assess empirical model estimations of GPH for each year of the recent California drought. We compare results from both the no lag and lag models using observed SIE/SST conditions from December–March and September–November 2013–2016, respectively.

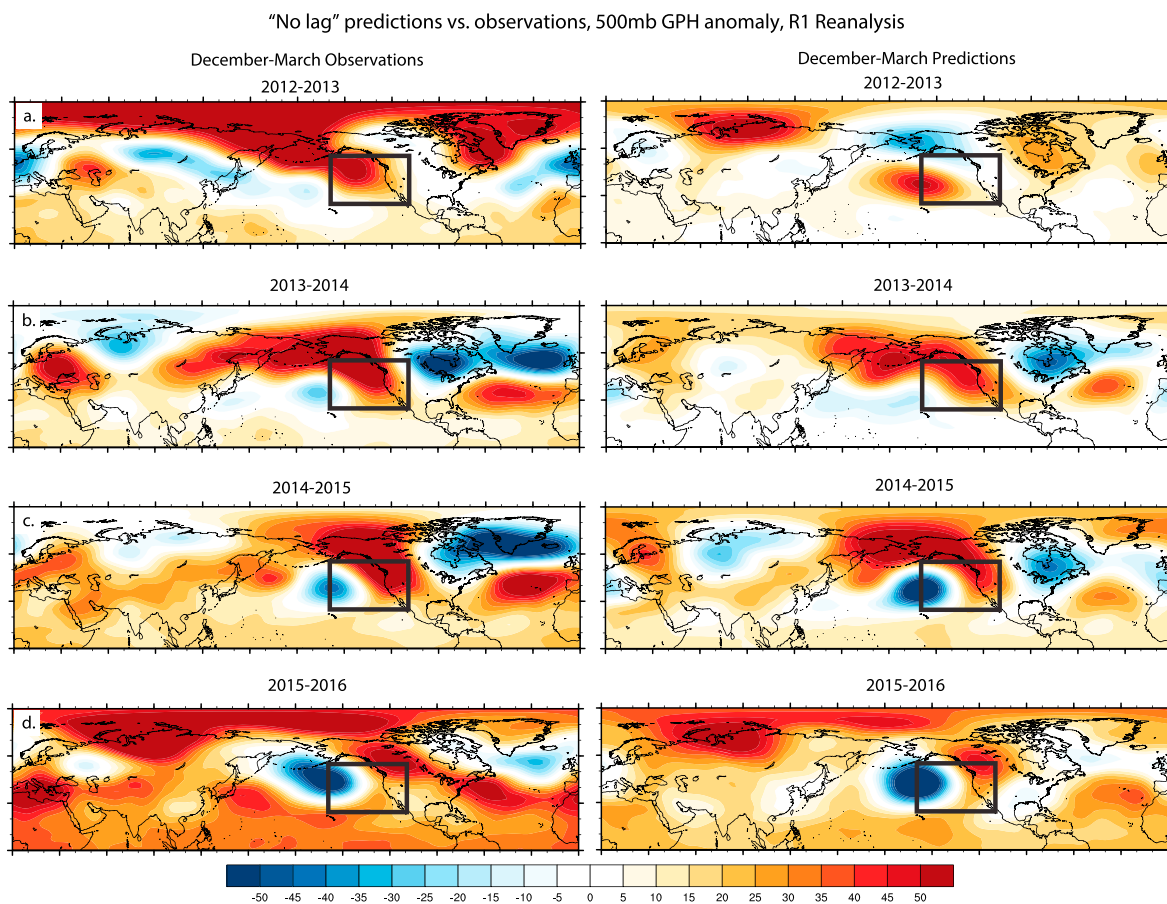


**Figure 6.** (a–d) Observed versus estimated December–March North Pacific ridging during the 2013–2016 California drought using the December–March no lag model. (left column) Observed 500 hPa geopotential height anomalies (m) for each December–March period between 2012–2013 and 2015–2016. (right column) Estimations (corresponding to panels at left) for California drought years using observed regressor values (see section 2). The black rectangles denote the northeasterly Pacific storm track region over which model skill (anomaly pattern correlation) is assessed.

#### 2.4. Data Sets, Definitions, and Statistical Tests

We obtain California December–March precipitation data from NOAA's Gridded Climate Divisional Dataset for the 1979–2016 period. We subdivide these precipitation data into percentile bins (interval = 10%).

We define the zonal tropical Pacific SST gradient as the absolute difference between the WP SST and EP SST, and the meridional Pacific SST gradient as the difference between EP SST and NEP SST.

All  $P$  values in this study are derived using a standard two-tailed  $t$  test. Adjusted  $R^2$  values are presented instead of standard  $R^2$ . We note that  $R^2$  values are generally larger in the tropics than midlatitudes but exhibit a pronounced regional maximum in the Pacific storm track region west of California.

While multicollinearity does not (in general) bias regression coefficient estimates, it can increase the variance of coefficient estimates, thereby increasing the likelihood of failure to detect a statistically significant effect (Mansfield & Helms, 1982). Therefore, we present information regarding the pairwise correlation structure and the variance inflation factor (VIF) associated with each regressor (Figure S3). The VIF is a measure of multicollinearity, with values  $\geq 10$  suggestive of strong multicollinearity (e.g., Belsley, Kuh, & Welsch, 2005). We note that the largest VIF is 5.47 for the "year term" regressor (Figure S3c), which is a product of correlated long-term trends in BK SIE, BC SIE, and WP SST, and is suggestive of moderate collinearity. As the SIE/SST regressors themselves exhibit relatively low multicollinearity ( $VIF \leq 4$ ; Figure S3c), we determine that the modest multicollinearity observed among the Earth system variables under consideration is acceptably low for the purposes of our analysis.

### 3. Results and Discussion

#### 3.1. North Pacific Atmospheric Circulation Associated With SST/Sea Ice Anomalies

We find strong observational relationships between seasonal-scale ocean conditions and North Pacific atmospheric pressure patterns for all three SST regions, with weaker links to SIE (Figure 1). Regression coefficients for each regressor exhibit considerable diversity of spatial patterns across the Northern Hemisphere, but here we focus on each regressor's contribution to positive North Pacific GPH anomalies ("ridging"). In the following discussion, all references to GPH refer to December–March values, December–March SIE/SST references refer to results from the no lag model, and references to September–November SIE/SST references refer to results from the lag model.

Warm NEP SSTs in December–March are associated with a wave-like pattern of December–March GPH, with positive values near western North America (including Alaska) and negative values to the east and west (Figure 1c). This southwest-northeast oriented pattern is reminiscent of the pronounced GPH dipole discussed in (Wang et al., 2015, 2014), which is thought to be linked to an ENSO-precursor SST pattern. Warm NEP SSTs in September–November are associated with a similar wave-like GPH pattern over North America in December–March, though with slightly weaker ridging along the West Coast (Figure S1c).

Cool (warm) EP SSTs in December–March coincide with strongly positive (negative) GPH anomalies across a broad swath of the North Pacific (Figure 1e), which likely reflects a weakening (strengthening) of the semipermanent Gulf of Alaska low associated with La Niña (El Niño) conditions (Alexander et al., 2002). A nearly identical December–March pattern emerges using September–November SSTs in the lag model (Figure S1e).

Warm WP SSTs coincide with a broad region of positive GPH anomalies over and west of California (Figure 1d), consistent with previously identified connections between enhanced West Pacific tropical convection and North Pacific ridging (Hartmann, 2015; Seager & Henderson, 2016; Teng & Branstator, 2016; Wang et al., 2014). As with NEP SST and EP SST, the lagged (September–November) relationship with December–March GPH is strikingly similar with the contemporaneous (December–March) relationship (Figure 1d)—offering observational evidence for statistical linkages persisting on multimonth timescales for all three Pacific SST regressors.

Low (high) SIE during December–March in both the BK and BC regions cooccurs with increased (decreased) December–March GPH over the far northeastern Pacific (Figures 1a and 1b), although the magnitude of the relationship is larger for BK SIE. While interactions between sea ice and midlatitude weather remain an active area of study (e.g., Cohen et al., 2014; Francis & Vavrus, 2012; Overland et al., 2016; Screen et al., 2014), a growing body of evidence suggests that sea ice loss can force zonally asymmetric GPH patterns across the Pacific/North American sector (Kug et al., 2015; Lee et al., 2015; Overland et al., 2016; Pedersen et al., 2016), and these linkages may occur via time-lagged troposphere-stratosphere interactions (Cohen et al., 2014; Zhang et al., 2016). In light of this, it is interesting to note that the observed relationships are substantially different for lagged (September–November) and nonlagged (December–March) SIE values. While BK SIE yields a similar (but weaker) GPH pattern in both cases (Figure S1a versus Figure 1a), the lagged GPH anomaly pattern associated with low BC SIE in autumn is actually greater in magnitude than that associated with winter BK SIE (Figure S1b versus Figure 1b).

We test whether these observational relationships between remote influences and atmospheric pressure patterns are consistent with those that arise in the NCAR CESM Large Ensemble Experiment (NCAR CESM-LE; see section 2). We find striking similarity between observed and simulated pressure patterns over the northeastern Pacific for all three contemporaneous SST regressors (Figures 1a–1e versus Figures 2a–2e), with warm WP SSTs yielding a broad region of subtropical ridging centered southwest of California and cool EP SSTs yielding atmospheric ridging over the Gulf of Alaska. Warm NEP SSTs coincide with a familiar "wave-like" GPH anomaly pattern extending from the central North Pacific to eastern North America. In the no lag model, the ensemble mean spatial pattern of GPH over the northeastern Pacific is highly similar (pattern correlation  $\geq 0.7$ ) to that of individual ensemble members in 27 of 28 realizations for WP SSTs, 20 of 28 realizations for EP SSTs, and 24 of 28 realizations for NEP SSTs (Figure 3c) in the no lag model. This strong clustering (particularly for WP and NEP SST) in a large coupled climate model ensemble indicates that the relationships between regional SST and northeastern Pacific atmospheric circulation have a strong physical basis. Further, the congruence of these

simulated patterns with those arising in observations suggests that these SST-GPH relationships are likely a robust feature of the real-world climate system.

The interpretation of NEP SST-linked spatial patterns is complicated by the difference between the CESM-based results in the lag and no lag analyses. Strong and spatially similar contemporaneous SST/GPH linkages exist in both the reanalysis and CESM-based analyses (Figures 1c and 2c). However, while such a “West Coast ridge” pattern also emerges using lagged autumn NEP SSTs from reanalysis (Figure S1c), it does not appear in the lagged CESM ensemble-mean analysis (Figure S2c). We suggest two possible reasons for this divergence. First, if warm NEP SSTs have been caused primarily by the presence of inhibited ocean mixing caused by pre-existing ridging (e.g., Bond et al., 2015), the SSTs themselves would likely exhibit little lead/lag relationship prior to the development of positive GPH anomalies—in which case, the observed lagged relationship could have occurred by chance. Second, it is possible that the coupled GCM simulations do not adequately capture ocean-atmosphere coupling in this extratropical region on longer timescales (e.g., Fang & Yang, 2016)—a situation that may be indicated by the existence of a statistically significant lagged NEP SST/GPH relationship in reanalysis but not in CESM. In either case, it is also plausible that self-reinforcing ocean-atmosphere feedback between locally warm SSTs and the nearby ridge are simply occurring on subseasonal timescales (i.e., on a weekly or monthly basis within the December–March period).

In contrast to SST relationships, however, the observed relationships between sea ice and North Pacific ridging are not present in the CESM ensemble mean. While similar high-latitude GPH anomaly patterns arise in both observational and model-based no lag analyses, we find little overall midlatitude GPH signal in the CESM ensemble mean for BK SIE (Figure 2a versus Figure 1a) and a North Pacific GPH anomaly pattern of opposite in sign as the reanalysis for BK SIE (Figure 2b versus Figure 1b). In the lagged CESM ensemble-mean analysis, there is very little GPH signal anywhere in the Northern Hemisphere (Figures S2a and S2b). We reiterate, however, that these findings do not necessarily constitute a negative result. It is plausible that the most relevant timescale for SIE/GPH relationships is shorter than the interseasonal timescale presumed by a September–November to December–March lag and that the “contemporaneous” results presented in Figures 1 and 2 may mask sea ice-atmosphere linkages occurring on weekly to monthly timescales.

Further analysis of individual model ensemble members also reveals that the weak ensemble-mean relationship between SIE and midlatitude GPH is not necessarily representative of the relationship in individual realizations—and may result from the “smoothing” effect of averaging spatially divergent patterns across the large ensemble. The GPH relationship to BC SIE anomalies is highly variable across individual ensemble members, with few (3 of 28) individual members exhibiting a GPH pattern highly similar to the ensemble mean (Figure 3c). In the case of BK SIE, slightly over half of the individual ensemble members (18 of 28) exhibit a GPH pattern that is highly similar to the ensemble mean (Figure 3c). The fact that individual realizations show strong (but sometimes opposing) GPH anomaly patterns associated with SIE anomalies, but the climate model exhibits a weak signal in the ensemble mean, supports previously published arguments that relationships between Arctic sea ice and midlatitude circulation may depend on the background state of the coupled ocean-atmosphere system and/or may project strongly onto other modes of variability (e.g., Blackport & Kushner, 2017; Overland et al., 2016; Screen et al., 2014).

Either of these conditions could potentially explain the wide range of simulated relationships that we report across the many realizations of a single physical model. However, we add as a significant caveat that systematic errors in CESM could also prevent accurate representation of these Earth system interactions. For example, emerging evidence suggests that interactions between Arctic surface conditions and midlatitude atmospheric circulation likely involve time-lagged troposphere-stratosphere interactions (e.g., Cohen et al., 2014; Zhang et al., 2016), which may not be adequately resolved by CESM. Moreover, in contrast to our CESM-related findings, Kim et al. (2014) report a robust North Pacific early winter atmospheric response to Barents-Kara sea ice loss using a different atmospheric model and experimental design—suggesting that intermodel differences (and related biases in troposphere-stratosphere interactions) can substantially affect the simulated sea ice relationships.

We also note the occurrence of a small region of modest but statistically significant ( $p < 0.10$ ) regression coefficients near California associated with BC ice in the no lag CESM analysis (Figure 2b). The sign of this simulated relationship is opposite to that in observations (in the CESM simulations, reduced sea ice in the

BC region is associated with lower geopotential heights near California, as opposed to ridging in the reanalysis-based regression; Figure 2b versus Figure 1b)—suggesting that low BC SIE conditions are associated with a weaker winter mean ridge along the West coast and “flattened” zonal flow in CESM. Interestingly, Blackport & Kushner (2017) report a spatially similar but much stronger relationship between basin-wide reductions in Arctic sea ice, decreased geopotential heights over the northeastern Pacific, and increased precipitation over California. The simulated reductions in sea ice examined by Blackport & Kushner (2017) are much larger than those which occur during the 1920–2005 CESM-LE simulations, so it is plausible that the forced signal in our analysis is simply too small to produce the same magnitude of response.

Despite these sea ice-related uncertainties, our observational and modeling results agree that anomalous Pacific SSTs coincide with an increased likelihood of northeastern Pacific ridging (Figures 1, 2, S1, and S2). Since climate models are frequently better able to simulate regional-scale atmospheric circulation extremes than precipitation extremes themselves (e.g., Schroeder et al., 2016), knowledge of SST configurations that are conducive to Pacific ridging has the potential to yield increased predictability of California precipitation extremes. The enhanced predictive power of regional-scale circulation has recently been leveraged in a hybrid statistical-dynamical modeling framework to improve seasonal precipitation forecasts for the American Southwest (Madadgar et al., 2016) and used in a “pattern analogue” approach to better characterize changes in heavy precipitation events along the western coast of North America (Gao et al., 2016). In the present study, we find that the reanalysis-based empirical model explains a large fraction (>50% for the no lag model; >40% for the lag model) of the year-to-year variance in both GPH in the region and immediately to the southwest of California (Figure 5)—despite the fact that this region is characterized by large interannual variability (e.g., Seager et al., 2015).

### 3.2. Quantification of Model Performance

To test whether our empirical model can provide useful information regarding the occurrence of atmospheric circulation patterns similar to those during the California drought, we compare GPH estimated by our empirical statistical model to GPH that actually occurred. We find that both our lag and no lag statistical models reproduce key characteristics of the observed northeastern Pacific GPH pattern during each season between 2012–2013 and 2015–2016, including (1) a broad area of anomalously positive GPH in 2012–2013 (Figures 6a and S4a) and (2) an amplified North Pacific trough/ridge “dipole” pattern during 2013–2014, 2014–2015, and 2015–2016 (Figures 6b–6d and S4b–S4d). Further, the empirical model captures a subtle eastward shift of this persistent wave-like anomaly pattern over successive seasons (Figures 6b–6d and S4b–S4d), which ultimately had large implications for West Coast precipitation (Swain et al., 2016) and East Coast cold temperature extremes (Singh et al., 2016). Overall, we find that although the absolute magnitude of the estimated GPH anomalies is underestimated (Figures 6 and S4), estimated spatial patterns over the northeastern Pacific are highly similar to those observed during the California drought (mean pattern correlation during 2013–2016 = 0.69 using the no lag model and 0.54 using the lag model) (Figure 4).

Over the full 1979–2016 period, we find that the empirical model estimates spatial patterns of December–March GPH that exhibit moderate to high ( $\geq 0.4$ ) pattern correlation with observations for 66% of years using the no lag model and 48% of years using the lag model (Figure 4). A significant fraction of specific years substantially exceed this benchmark (with high pattern correlation ( $\geq 0.6$ ) for 40% (37%) of years exhibited by the no-lag (lag) model). Results from both cross-validation procedures suggest that this correlation is not highly sensitive to the exclusion of training data. In particular, empirical models generated using both the “leave one out” and “leave four out” methods yield mean GPH pattern correlations exceeding the 0.4 benchmark for 2013–2016 drought years that are the focus of this manuscript—even when these years are completely excluded from the training set (Figure 4). We also show in Figures S5 and S6 (versus Figures 1 and S1) that the exclusion of 2013–2016 data does not substantially affect the spatial pattern or magnitude of standardized regression coefficients for either the no lag or lag model.

We emphasize that the ability of the empirical model to reproduce the observed GPH pattern in a majority of cases is not trivial—especially in a region characterized by large natural variability. While there are a number of years where the empirical model exhibits low (or even negative) skill in reproducing observed GPH patterns, this result is not especially surprising in light of the large internal variability of the

ocean-atmosphere system. Recent work has pointed out that random variability may indeed be a primary driver of observed North Pacific GPH variability in specific years (Seager et al., 2015; Teng & Branstrator, 2016)—a contribution which even a perfect empirical model would be unable to capture. Nevertheless, our finding that the lagged model yields comparable results to the no lag model suggests that there is “memory” in the coupled ocean-atmosphere system that persists on multimonth timescales. In particular, this result suggests that autumn SSTs in the Pacific may indeed offer a meaningful degree of foresight regarding winter GPH in the storm track region relevant for California cool-season precipitation.

### 3.3. Findings in Context of Anthropogenically Forced Trends in SST/Sea Ice

Our findings can be interpreted in a broader climatological context. Between 1979 and 2012, SIE exhibits strong decreasing trends during September–November for BK and BC (Figures S1a and S1b) and during December–March for BK SIE (Figure 1a), consistent with greenhouse gas-forced CESM simulations (Figures 2a and 2b and S2a and S2b). WP SST, meanwhile, exhibits an increasing trend (Figure 1d) during both September–November and December–March, also consistent with simulations (Figures 2d and S2d). However, despite extremely warm observed values since 2013, neither NEP nor EP SST exhibits statistically significant trends in September–November or December–March (Figures 1c and 1e and S1c and S1d)—in contrast to CESM simulations, which exhibit statistically significant warming (except for NE Pac SST in September–November; Figures 2c and 2e and S2c and S2e). This divergence between observed and simulated regional SSTs has previously been linked to the persistently “La Niña-like” state observed in the tropical Pacific (Medhaug et al., 2017), which modulated global temperature trends and influenced Northern Hemisphere precipitation patterns (Funk & Hoell, 2015).

Consistent with earlier findings by Hoell and Funk (2013), we report stronger zonal tropical Pacific SST gradient over the 1979–2016 period ( $p = 0.07$ ), in addition to a weakened meridional SST gradient ( $p = 0.13$ ) (Figure 3b). Known teleconnections between tropical Pacific SST gradients and midlatitude atmospheric circulation (Hoell & Funk, 2013), combined with the potential for meridional SST gradients to influence the strength/position of the Pacific storm track (Brayshaw, Hoskins, & Blackburn, 2008), suggest that these changing SST gradients may have increased the propensity for northeastern Pacific ridging in recent years (Swain et al., 2016). Finally, we emphasize that while several remote regressors reached record-high (NEP and EP SST) or record-low (BK SIE) values over the course of the 2013–2016 drought, previous California dry spells have coincided with a wide range of SIE/SST conditions (Figure 3a). Therefore, there are likely multiple combinations of remote conditions that can interact to enhance or reduce the probability of atmospheric patterns conducive to California drought.

### 3.4. Caveats Regarding Overall Approach

We reiterate that fully disambiguating the complex and potentially interacting Earth system processes linking remote regional influences to high-impact atmospheric circulation regimes will require targeted numerical experiments that capture the spatiotemporal complexity of North Pacific climate. Our primary goal in constructing a physically interpretable statistical model is to assess the character and spatial patterns of contemporaneous relationships between SST/sea ice and atmospheric conditions, with a focus on understanding previously hypothesized linkages during the 2013–2016 California drought in particular.

We acknowledge, however, that real-world relationships are unlikely to be strictly linear (Overland et al., 2016; Screen, 2017; Shepherd, 2014) and may in fact be state-dependent (Overland et al., 2016). Additionally, our methods allow us to infer associative linkages—rather than demonstrate the directionality of causal relationships—between SST/sea ice and atmospheric circulation. Thus, further work aimed at elucidating underlying physical mechanisms is necessary. We emphasize that uncertainties regarding the robustness of relationships in the relatively short observational record and the ability of coupled climate models to correctly simulate relevant SST/sea ice feedback highlight the challenge of systematically diagnosing Earth system relationships in a complex and nonstationary climate system.

Finally, we acknowledge the challenge of disambiguating relationships between nonstationary variables that exhibit nontrivial collinearity. While our systematic cross-validation procedure suggests that the regressions are robust, we cannot exclude the possibility that multiple regressors are in fact common responses to another driver not accounted for in our analyses.

#### 4. Conclusions

We have developed an observation-based empirical model intended to isolate connections between several potential remote regressors and North Pacific atmospheric conditions. We confirm the robustness of Pacific SST-related relationships using climate model simulations but find greater uncertainty in the robustness of sea ice linkages. In agreement with previous work linking warmth in the western tropical Pacific Ocean to the California drought (e.g., Seager et al., 2015; Seager & Henderson, 2016), we also find lagged ocean-atmosphere relationships on seasonal timescales that may represent an important source of foresight regarding anomalous North Pacific ridging. Ultimately, we find that this parsimonious empirical model does indeed reproduce the spatial pattern of anomalous North Pacific high pressure during the 2012–2016 California drought, even when autumn SST/SIE conditions are used to estimate winter GPH (although we acknowledge that the extreme magnitude of the observed ridge is underestimated). Collectively, these findings strongly suggest that the California drought can be at least partially traced to coupled Earth system processes but also reinforce the notion that multiple aggravating factors were likely at play—including internal variability and possibly other ocean, sea ice, or land surface conditions not considered in this study.

We find that historically forced climate model simulations depict substantial long-term trends in nearly all examined SST and sea ice regions, highlighting the potential for continued greenhouse gas emissions to affect SST and sea ice patterns that have historically been connected to North Pacific ridging (and consequently to the risk of California drought). Our results suggest that the specific spatial patterns of future ocean warming—about which there remains considerable uncertainty—may be highly consequential for California's future climate.

Recent events further underscore the relevance of these findings. The 2015–2016 El Niño event, which was among the strongest in the observational record, failed to bring widely anticipated drought relief to much of California—particularly in the south, where the historical relationship between ENSO and precipitation is typically strongest (Hoell et al., 2016). The lack of drought relief in California can be proximally linked to the persistence of subtropical ridging to the southwest of the state, which redirected the strong Pacific jet stream northward and instead brought record precipitation to the Pacific Northwest. The empirical model developed in this study largely reproduces the spatial pattern (if not the full magnitude) of the observed atmospheric anomalies during this period. We suggest therefore that the unusual character of the regional atmospheric response to ENSO may have been foreseeable with sufficient knowledge of regional SST/sea ice conditions.

Contrarily, widespread and substantial drought relief subsequently occurred in California during late 2016 and early 2017 amidst an extended period of persistent storminess and near-record precipitation (United States Drought Monitor via <http://droughtmonitor.unl.edu>). These wet conditions occurred despite the lack of a well-defined La Niña or El Niño event in the Pacific Ocean. While Pacific Ocean temperatures were not particularly anomalous relative to recent extreme years (NOAA Earth System Research Laboratory (ESRL) Map Room via <https://www.esrl.noaa.gov/psd/map/clim/sst.shtml>), regional Arctic sea ice exhibited record-low extent during the autumn and early winter of 2016–2017, especially in the Barents/Kara and Bering/Chukchi sectors (National Snow and Ice Data Center Arctic Sea Ice News and Analysis via <https://nsidc.org/arcticseaicenews>). These informal observations further underscore the potential importance of teleconnections between geographically remote regional processes and North Pacific large-scale circulation patterns capable of producing both dry and wet extremes. We suggest that there may be promise in refining these relationships in pursuit of improved real-time predictions of seasonal precipitation—and subsequent drought and flood risk—in California.

#### Data Availability

GPH data from the NCEP R1 Reanalysis are available from the NOAA ESRL website ([www.esrl.noaa.gov/psd/data/gridded/data.ncep.reanalysis.html](http://www.esrl.noaa.gov/psd/data/gridded/data.ncep.reanalysis.html)). SST data from the ERSSTv4 analysis are also available from the NOAA ESRL website (<http://www.esrl.noaa.gov/psd/data/gridded/data.noaa.ersst.v4.html>). SIE data from the HadISST analysis are available from the Hadley Center website (<http://www.metoffice.gov.uk/hadobs/hadisst>). GPH, SST, and SIE data from the LENS simulations are available from UCAR (<http://www.cesm.ucar.edu/projects/community-projects/LENS/data-sets.html>). Precipitation data for California are

available from the NOAA NCDC Web site ([www.ncdc.noaa.gov/monitoring-references/maps/us-climate-divisions.php](http://www.ncdc.noaa.gov/monitoring-references/maps/us-climate-divisions.php)). Code used in the analyses described in the paper may be obtained upon request by contacting the corresponding author.

### Competing Financial Interests

The authors declare that they have no competing financial interests.

### Acknowledgments

Our work was supported by a Robert and Patricia Switzer Foundation Fellowship, an Achievement Rewards for College Scientists Foundation Fellowship, and a Nature Conservancy NatureNet Fellowship awarded to D.L.S.; a G. J. Lieberman Fellowship and a Lamont-Doherty Earth Observatory Fellowship awarded to D.S.; an Earth Institute Fellowship to J.S.M; and an NSF AGS CAREER grant 0955283 and U.S. Department of Energy Integrated Assessment Research Program grant DE-SC005171 awarded to N.S.D. Additional support was provided to D.L.S. by the UCLA Sustainable LA Grand Challenge.

### References

- Alexander, M. A., Bladé, I., Newman, M., Lanzante, J. R., Lau, N.-C., & Scott, J. D. (2002). The atmospheric bridge: The influence of ENSO teleconnections on air-sea interaction over the global oceans. *Journal of Climate*, 15(16), 2205–2231. [https://doi.org/10.1175/1520-0442\(2002\)015%3C2205:tatbio%3E2.0.co;2](https://doi.org/10.1175/1520-0442(2002)015%3C2205:tatbio%3E2.0.co;2)
- Asner, G. P., Brodrick, P. G., Anderson, C. B., Vaughn, N., Knapp, D. E., & Martin, R. E. (2016). Progressive forest canopy water loss during the 2012–2015 California drought. *Proceedings of the National Academy of Sciences of the United States of America*, 113(2), E249–E255. <https://doi.org/10.1073/pnas.1523397113>
- Belmecheri, S., Babst, F., Wahl, E. R., Stahle, D. W., & Trouet, V. (2016). Multi-century evaluation of Sierra Nevada snowpack. *Nature Climate Change*, 6(1), 2–3. <https://doi.org/10.1038/nclimate2809>
- Belsley, D. A., Kuh, E., & Welsch, R. E. (2005). *Regression diagnostics: Identifying influential data and sources of collinearity*. John Wiley & Sons.
- Blackport, R., & Kushner, P. J. (2017). Isolating the atmospheric circulation response to Arctic sea ice loss in the coupled climate system. *Journal of Climate*, 30(6), 2163–2185. <https://doi.org/10.1175/JCLI-D-16-0257.1>
- Bond, N. A., Cronin, M. F., Freeland, H., & Mantua, N. (2015). Causes and impacts of the 2014 warm anomaly in the NE Pacific. *Geophysical Research Letters*, 42(9), 3414–3420. <https://doi.org/10.1002/2015GL063306>
- Brayshaw, D. J., Hoskins, B., & Blackburn, M. (2008). The storm-track response to idealized SST perturbations in an Aquaplanet GCM. *Journal of the Atmospheric Sciences*, 65, 2842–2860. <https://doi.org/10.1175/2008JAS2657.1>
- Cayan, D., & Roads, J. (1984). Local relationships between United-States West-Coast precipitation and monthly mean circulation parameters. *Monthly Weather Review*, 112(6), 1276–1282. [https://doi.org/10.1175/1520-0493\(1984\)112%3C1276:LRBUSW%3E2.0.CO;2](https://doi.org/10.1175/1520-0493(1984)112%3C1276:LRBUSW%3E2.0.CO;2)
- Cohen, J., Screen, J. A., Furtado, J. C., Barlow, M., Whittlestone, D., Coumou, D., ... Jones, J. (2014). Recent Arctic amplification and extreme mid-latitude weather. *Nature Geoscience*, 7(9), 627–637. <https://doi.org/10.1038/ngeo2234>
- Deser, C., Phillips, A. S., Alexander, M. A., & Smoliak, B. V. (2014). Projecting North American climate over the next 50 years: Uncertainty due to internal variability. *Journal of Climate*, 27(6), 2271–2296. <https://doi.org/10.1175/jcli-d-13-00451.1>
- Diffenbaugh, N., Swain, D., & Touma, D. (2015). Anthropogenic warming has increased drought risk in California. *Proceedings of the National Academy of Sciences of the United States of America*, 112(13), 3931–3936. <https://doi.org/10.1073/pnas.1422385112>
- Di Lorenzo, E., & Mantua, N. (2016). Multi-year persistence of the 2014/15 North Pacific marine heatwave. *Nature Climate Change*, 6(11), 1042–1047. <https://doi.org/10.1038/nclimate3082>
- Fang, J., & Yang, X.-Q. (2016). Structure and dynamics of decadal anomalies in the wintertime midlatitude North Pacific ocean-atmosphere system. *Climate Dynamics*, 47(5–6), 1989–2007. <https://doi.org/10.1007/s00382-015-2946-x>
- Francis, J. A., & Vavrus, S. J. (2012). Evidence linking Arctic amplification to extreme weather in mid-latitudes. *Geophysical Research Letters*, 39, L06801. <https://doi.org/10.1029/2012GL051000>
- Funk, C., Hoell, A., & Stone, D. (2014). Examining the contribution of the observed global warming trend to the California droughts of 2012/13 and 2013/14. *Bulletin of the American Meteorological Society*, 95(9), S11–S15.
- Funk, C. C., & Hoell, A. (2015). The leading mode of observed and CMIP5 ENSO-residual Sea surface temperatures and associated changes in Indo-Pacific climate. *Journal of Climate*, 28(11), 4309–4329. <https://doi.org/10.1175/JCLI-D-14-00334.1>
- Gan, B., & Wu, L. (2012). Modulation of atmospheric response to North Pacific SST anomalies under global warming: A statistical assessment. *Journal of Climate*, 25, 6554–6566. <https://doi.org/10.1175/jcli-d-11-00493.1>
- Gao, X., Schlosser, C. A., O'Gorman, P., Monier, E., & Entekhabi, D. (2016). 21st century changes in U.S. regional heavy precipitation frequency based on resolved atmospheric patterns. *Journal of Climate*, 30(7), 2501–2521. <https://doi.org/10.1175/JCLI-D-16-0544.1>
- Griffin, D., & Anchukaitis, K. J. (2014). How unusual is the 2012–2014 California drought? *Geophysical Research Letters*, 41(24), 9017–9023. <https://doi.org/10.1002/2014GL062433>
- Hartmann, D. L. (2015). Pacific sea surface temperature and the winter of 2014. *Geophysical Research Letters*, 42(6), 1894–1902. <https://doi.org/10.1002/2015GL063083>
- Hoell, A., & Funk, C. (2013). The ENSO-related West Pacific sea surface temperature gradient. *Journal of Climate*, 26(23), 9545–9562. <https://doi.org/10.1175/JCLI-D-12-00344.1>
- Hoell, A., Hoerling, M., Eischeid, J., Wolter, K., Dole, R., Perlitz, J., ... Cheng, L. (2016). Does El Niño intensity matter for California precipitation? *Geophysical Research Letters*, 43(2), 819–825. <https://doi.org/10.1002/2015GL067102>
- Horton, D., Johnson, N., Singh, D., Swain, D., Rajaratnam, B., & Diffenbaugh, N. (2015). Contribution of changes in atmospheric circulation patterns to extreme temperature trends. *Nature*, 522(7557), 465–469. <https://doi.org/10.1038/nature14550>
- Huang, B., Banzon, V. F., Freeman, E., Lawrimore, J., Liu, W., Peterson, T. C., ... Zhang, H.-M. (2014). Extended Reconstructed Sea Surface Temperature Version 4 (ERSST.v4). Part I: Upgrades and intercomparisons. *Journal of Climate*, 28(3), 911–930. <https://doi.org/10.1175/JCLI-D-14-00006.1>
- Jeffries, K. M., Connon, R. E., Davis, B. E., Komoroske, L. M., Britton, M. T., Sommer, T., ... Fangue, N. A. (2016). Effects of high temperatures on threatened estuarine fishes during periods of extreme drought. *The Journal of Experimental Biology*, 219(11), 1705–1716. <https://doi.org/10.1242/jeb.134528>
- Kalnay, E., Kanamitsu, M., Kistler, R., Collins, W., Deaven, D., Gandin, L., ... Joseph, D. (1996). The NCEP/NCAR 40-year reanalysis project. *Bulletin of the American Meteorological Society*, 77(3), 437–471. [https://doi.org/10.1175/1520-0477\(1996\)077%3C437:tncrp%3E2.0.co;2](https://doi.org/10.1175/1520-0477(1996)077%3C437:tncrp%3E2.0.co;2)
- Kay, J. E., Deser, C., Phillips, A., Mai, A., Hannay, C., Strand, G., ... Vertenstein, M. (2015). The Community Earth System Model (CESM) Large Ensemble Project: A community resource for studying climate change in the presence of internal climate variability. *Bulletin of the American Meteorological Society*, 96(8), 1333–1349. <https://doi.org/10.1175/bams-d-13-00255.1>
- Kim, B.-M., Son, S.-W., Min, S.-K., Jeong, J.-H., Kim, S.-J., Zhang, X., ... Yoon, J.-H. (2014). Weakening of the stratospheric polar vortex by Arctic sea-ice loss. *Nature Communications*, 5, 4646. <https://doi.org/10.1038/ncomms5646>

- Kug, J.-S., Jeong, J.-H., Jang, Y.-S., Kim, B.-M., Folland, C. K., Min, S.-K., & Son, S.-W. (2015). Two distinct influences of Arctic warming on cold winters over North America and East Asia. *Nature Geoscience*, 8(10), 759–762. <https://doi.org/10.1038/ngeo2517>
- Lee, M.-Y., Hong, C.-C., & Hsu, H.-H. (2015). Compounding effects of warm sea surface temperature and reduced sea ice on the extreme circulation over the extratropical North Pacific and North America during the 2013–2014 boreal winter. *Geophysical Research Letters*, 42(5), 1612–1618. <https://doi.org/10.1002/2014GL062956>
- Madadgar, S., AghaKouchak, A., Shukla, S., Wood, A. W., Cheng, L., Hsu, K. L., & Svoboda, M. (2016). A hybrid statistical-dynamical framework for meteorological drought prediction: Application to the southwestern United States. *Water Resources Research*, 52(7), 5095–5110. <https://doi.org/10.1002/2015WR018547>
- Mansfield, E. R., & Helms, B. P. (1982). Detecting multicollinearity. *The American Statistician*, 36(3), 158–160. <https://doi.org/10.2307/2683167>
- Medhaug, I., Stolpe, M. B., Fischer, E. M., & Knutti, R. (2017). Reconciling controversies about the ‘global warming hiatus’. *Nature*, 545(7652), 41–47. <https://doi.org/10.1038/nature22315>
- Overland, J. E., Dethloff, K., Francis, J. A., Hall, R. J., Hanna, E., Kim, S.-J., ... Vihma, T. (2016). Nonlinear response of mid-latitude weather to the changing Arctic. *Nature Climate Change*, 6(11), 992–999. <https://doi.org/10.1038/nclimate3121>
- Pedersen, R. A., Cvijanovic, I., Langen, P. L., & Vinther, B. M. (2016). The impact of regional Arctic sea ice loss on atmospheric circulation and the NAO. *Journal of Climate*, 29(2), 889–902. <https://doi.org/10.1175/JCLI-D-15-0315.1>
- Rayner, N. A., Parker, D. E., Horton, E. B., Folland, C. K., Alexander, L. V., Rowell, D. P., ... Kaplan, A. (2003). Global analyses of sea surface temperature, sea ice, and night marine air temperature since the late nineteenth century. *Journal of Geophysical Research*, 108, 4407. <https://doi.org/10.1029/2002JD002670>
- Robeson, S. (2015). Revisiting the recent California drought as an extreme value. *Geophysical Research Letters*, 42(16), 6771–6779. <https://doi.org/10.1002/2015GL064593>
- Santer, B. D., Bonfils, C., Painter, J. F., Zelinka, M. D., Mears, C., Solomon, S., ... Wentz, F. J. (2014). Volcanic contribution to decadal changes in tropospheric temperature. *Nature Geoscience*, 7(3), 185–189. <https://doi.org/10.1038/ngeo2098>
- Schroeder, M., Wang, S.-Y. S., Gillies, R. R., & Hsu, H.-H. (2016). Extracting the tropospheric short-wave influences on subseasonal prediction of precipitation in the United States using CFSv2. *Climate Dynamics*, 48(11–12), 3967–3974. <https://doi.org/10.1007/s00382-016-3314-1>
- Screen, J. A. (2017). Simulated atmospheric response to regional and Pan-Arctic sea-ice loss. *Journal of Climate*, 30(11), 3945–3962. <https://doi.org/10.1175/JCLI-D-16-0197.1>
- Screen, J. A., Deser, C., Simmonds, I., & Tomas, R. (2014). Atmospheric impacts of Arctic sea-ice loss, 1979–2009: Separating forced change from atmospheric internal variability. *Climate Dynamics*, 43(1–2), 333–344. <https://doi.org/10.1007/s00382-013-1830-9>
- Seager, R., & Henderson, N. (2016). On the role of tropical ocean forcing of the persistent North American West Coast ridge of winter 2013/14. *Journal of Climate*, 29(22), 8027–8049. <https://doi.org/10.1175/JCLI-D-16-0145.1>
- Seager, R., Hoerling, M., Schubert, S., Wang, H., Lyon, B., Kumar, A., ... Henderson, N. (2015). Causes of the 2011–14 California drought\*. *Journal of Climate*, 28(18), 6997–7024. <https://doi.org/10.1175/jcli-d-14-00860.1>
- Shepherd, T. G. (2014). Atmospheric circulation as a source of uncertainty in climate change projections. *Nature Geoscience*, 7(10), 703–708. <https://doi.org/10.1038/ngeo2253>
- Shepherd, T. G. (2016). Effects of a warming Arctic. *Science*, 353(6303), 989–990. <https://doi.org/10.1126/science.aag2349>
- Singh, D., Swain, D. L., Mankin, J. S., Horton, D. E., Thomas, L. N., Rajaratnam, B., & Diffenbaugh, N. S. (2016). Recent amplification of the North American winter temperature dipole. *Journal of Geophysical Research: Atmospheres*, 121(17), 9911–9928. <https://doi.org/10.1002/2016JD025116>
- Swain, D. (2015). A tale of two California droughts: Lessons amidst record warmth and dryness in a region of complex physical and human geography. *Geophysical Research Letters*, 42(22), 9999–10,003. <https://doi.org/10.1002/2015GL066628>
- Swain, D., Horton, D., Singh, D., & Diffenbaugh, N. (2016). Trends in atmospheric patterns conducive to seasonal precipitation and temperature extremes in California. *Science Advances*, 2(4), e1501344. <https://doi.org/10.1126/sciadv.1501344>
- Swain, D., Tsiang, M., Haugen, M., Singh, D., Charland, A., Rajaratnam, B., & Diffenbaugh, N. (2014). The extraordinary California drought of 2013/2014: Character, context, and the role of climate change. *Bulletin of the American Meteorological Society*, 95(9), S3–S7.
- Teng, H., & Branstator, G. (2016). Causes of extreme ridges that induce California droughts. *Journal of Climate*, 30(4), 1477–1492. <https://doi.org/10.1175/JCLI-D-16-0524.1>
- Wang, H., & Schubert, S. (2014). Causes of the extreme dry conditions over California during early 2013. *Bulletin of the American Meteorological Society*, 95(9), S7–S11.
- Wang, S. Y., Hipps, L., Gillies, R. R., & Yoon, J.-H. (2014). Probable causes of the abnormal ridge accompanying the 2013–2014 California drought: ENSO precursor and anthropogenic warming footprint. *Geophysical Research Letters*, 41(9), 3220–3226. <https://doi.org/10.1002/2014gl059748>
- Wang, S.-Y. S., Huang, W.-R., & Yoon, J.-H. (2015). The North American winter ‘dipole’ and extremes activity: A CMIP5 assessment. *Atmospheric Science Letters*, 16(3), 338–345. <https://doi.org/10.1002/asl2.565>
- Williams, A. P., Seager, R., Abatzoglou, J. T., Cook, B. I., Smerdon, J. E., & Cook, E. R. (2015). Contribution of anthropogenic warming to California drought during 2012–2014. *Geophysical Research Letters*, 42(16), 6819–6828. <https://doi.org/10.1002/2015GL064924>
- Yoon, J.-H., Kravitz, B., Rasch, P. J., Simon Wang, S.-Y., Gillies, R. R., & Hipps, L. (2015). Extreme fire season in California: A glimpse into the future? *Bulletin of the American Meteorological Society*, 96(12), S5–S9. <https://doi.org/10.1175/BAMS-D-15-00114.1>
- Yoon, J.-H., Wang, S. Y. S., Gillies, R. R., Kravitz, B., Hipps, L., & Rasch, P. J. (2015). Increasing water cycle extremes in California and in relation to ENSO cycle under global warming. *Nature Communications*, 6, 8657. <https://doi.org/10.1038/ncomms9657>
- Zhang, J., Tian, W., Chipperfield, M. P., Xie, F., & Huang, J. (2016). Persistent shift of the Arctic polar vortex towards the Eurasian continent in recent decades. *Nature Climate Change*, 6(12), 1094–1099. <https://doi.org/10.1038/nclimate3136>